Solution-processed highly bright and durable cesium lead halide perovskite light-emitting diodes

Wei, Zhanhua; Perumal, Ajay; Su, Rui; Sushant, Shendre; Xing, Jun; Zhang, Qing; Tan, Swee Tiam; Demir, Hilmi Volkan; Xiong, Qihua

2016

Wei, Z., Perumal, A., Su, R., Sushant, S., Xing, J., Zhang, Q., . . . Xiong, Q. (2016). Solution-processed highly bright and durable cesium lead halide perovskite light-emitting diodes. Nanoscale, 8(42), 18021-18026. doi:10.1039/C6NR05330K

https://hdl.handle.net/10356/140356

https://doi.org/10.1039/C6NR05330K

Journal Name

COMMUNICATION

Solution-processed Highly Bright and Durable Cesium Lead Halide Perovskite Light-emitting Diodes

Received 00th January 20xx,
Accepted 00th January 20xx

DOI: 10.1039/x0xx00000x

www.rsc.org/

Zhanhua We,[a,c,] Ajay Perumal,[b] Rui Su,[a] Shendre Sushant,[b] Jun Xing,[a] Qing Zhang,[a] Swee Tiam Tan,[b] Hilmi Volkan Demir,[b,*] and Qihua Xiong[a,*]*

Recently, $CsPbBr_3$ perovskites are emerging as very promising green emission materials for light-emitting diodes (LEDs) due to their high color purity, low cost and high photoluminescence quantum yield (PLQY). However, the corresponding LEDs performance is still low and far behind the $CH_3NH_3PbBr_3$, it is due to lack of proper perovskite film preparation methods and interfacial engineering. Herein, we report a highly bright and durable $CsPbBr_3$-based LEDs fabricated using a one-step solution method. The precursor solution is prepared by simply dissolving $CsPbBr_3$ powder and CsBr additive in dimethyl sulfoxide (DMSO). We find that the CsBr additive not only significantly enhances the PLQY but also induces directional crystal growth into micro-plates, forming a smooth perovskite film for LEDs. LEDs employed such high quality films show a high luminance of 7,276 cd m^{-2} and high color purity with a full width at half maximum of 18 nm. Furthermore, the as-fabricated LEDs reveal an outstanding ambient stability with a decent luminance output (> 100 cd m^{-2}, steady increase without any degradation trend) for at least 15 h under a constant driving current density (66.7 mA cm^{-2}). And we propose two reasons for this unique luminance increasing behavior: (1) the $CsPbBr_3$ perovskite is thermally stable and can survive from joule heat; (2) on the other hand, the joule heating will induce interface or crystalline film annealing, reduce device resistance and then enhance luminance output.

Inorganic/organic hybrid perovskites have emerged as a prominent light harvester for novel high efficiency solid-state solar cells, with a recent power conversion efficiency reported over 22 %.[1-3] Recently, perovskite materials are found to be ideal emission materials and intensely investigated as emission layers in light-emitting diodes (LEDs) due to low cost, color tunability, high photoluminescence quantum yield (PLQY) and narrow emission peak.[4-9] Recently, Lee *et al.* have successfully boosted the current efficiency (CE) of inorganic/organic perovskite ($CH_3NH_3PbBr_3$) LEDs to 42.9 cd A^{-1} late 2015, indicating that perovskite-based LEDs can be as efficient and promising as the commercial phosphorescent organic light-emitting diodes (OLEDs).[10, 11] Constrained by the materials traits, ambient stability is an equally important challenge for the further development of potential perovskite-based LEDs applications. However, there are very few works which reported the stability performance of perovskite-based LEDs,[4] it is even more challenging to address the long-term stability.

It is well known that in perovskite solar cells, the organic components in the classical inorganic/organic perovskite materials ($MAPbX_3$, MA = CH_3NH_3, X = Cl, Br and I) are very sensitive to moisture and heat, *i.e.*, poor humidity and thermal stability,[12-15] which may also induce poor stability in perovskite-based LEDs. Very recently, cation engineering for perovskite, such as adding formamidinium $(FA)^2$ or Cs[16-18] to replace MA, is found to be an effective strategy to improve thermal and humidity stability of perovskite solar cells. In other words, this kind of cation engineering (partial replacement) or even cation replacement (all inorganic perovskites) could be possibly beneficial to fabricating high performance perovskite LEDs with good stability.

Herein, we report an all-inorganic perovskite ($CsPbBr_3$) based LEDs with outstanding ambient stability, high brightness (7,276 cd m^{-2}) and color purity (full width at half maximum, FWHM, 18 nm), which excels benchmarking to previous reports.[4, 5, 19, 20] When the as-fabricated LED devices were driven with a constant current (corresponding to an initial luminance of around 100 cd m^{-2}), we observed unexpected luminance increase instead of degradation. In more detail, during the initial 15 h of test, the luminance grows from 100 cd m^{-2} to ~400 cd m^{-2}, indicating considerably stable performance, which is no doubt an important advance in developing practical perovskite-based LEDs for daily life.

[a] *Division of Physics and Applied Physics, School of Physical and Mathematical Sciences, Nanyang Technological University, Singapore 637371. Email: qihua@ntu.edu.sg*
[b] *Luminous! Centre of Excellence for Semiconductor Lighting and Displays, School of Electrical and Electronic Engineering, Nanyang Technological University, Singapore 639798. Email: hvdemir@ntu.edu.sg*
[c] *College of Materials Science & Engineering, Huaqiao University, Xiamen, Fujian, China 361021. Email: weizhanhua@hqu.edu.cn*
† *Z.H. Wei and A. Perumal contribute equally to this work.*
Electronic Supplementary Information (ESI) available: See DOI: 10.1039/x0xx00000x

One of the most attractive features of the inorganic/organic perovskite-based devices ($MAPbX_3$ and $FAPbX_3$) is their solution-processed capability. Thus, one can prepare a perovskite-based precursor solution with various recipes to achieve a high quality solid perovskite thin film by spin-coating or other methods.[21] In the past few years, the photovoltaic efficiency of perovskite devices increased rapidly by engineering the precursor solution, like solvent engineering[12, 22] and compositional engineering.[1, 2, 10] In other words, the recipe development of perovskite-based precursor solution plays a key role in pursuing highly efficient perovskite-based devices. However, due to the limited solubility of CsX (X = Cl, Br and I), one cannot prepare a transparent precursor solution by simply dissolving PbX_2 and CsX with certain solutions (N, N-Dimethylformamide (DMF), Dimethyl sulfoxide (DMSO) or their mixtures). To date, the advanced solution process engineering methods (single step methods) have not been applied to all inorganic perovskites. Alternatively, there are two methods developed recently to prepare all-inorganic perovskite thin films, *i.e.*, two-steps method[17, 23] and nanoparticle ink method.[24-26] The two-steps method is similar to the previously reported sequential deposition method for $CH_3NH_3PbI_3$ thin films,[27] *i.e.*, a $PbBr_2$ thin film is firstly prepared by spin-coating using $PbBr_2$-DMF solution, then the as-prepared $PbBr_2$ thin film is dripped in a hot CsX methanol solution and converted into $CsPbX_3$.[17,18] The nanoparticle ink method is to prepare $CsPbX_3$ nanocrystals (NCs) or quantum dots (QDs) firstly, then the perovskite thin films can be prepared by spin-coating using the as-prepared nanoparticles colloid solution.[24, 25] In this work, we showed that $CsPbBr_3$ thin film can be simply prepared via spin-coating using a one-step solution method, which is more controllable and convenient than the above two methods.

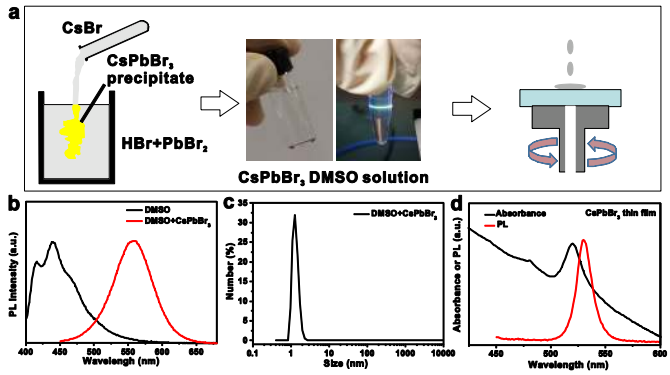

Figure 1. One-step solution-processed $CsPbBr_3$ thin films. (a) Schematic diagrams of preparing $CsPbBr_3$ powder (left), photographs of the corresponding transparent and colorless $CsPbBr_3$-DMSO solution illuminated by normal light and a blue laser of 405 nm (middle) and thin film deposition using spin-coating (right). (b) Photoluminescence (PL) spectra of DMSO and DMSO+$CsPbBr_3$ solution. (c) Dynamic light scattering spectroscopy of the DMSO+$CsPbBr_3$ solution. (d) UV-Vis absorption and PL spectrum of a $CsPbBr_3$ thin film prepared by the one-step spin-coating.

Figure 1a schematically shows the process of preparing $CsPbBr_3$ thin film by one-step spin-coating. First, $PbBr_2$ powder was dissolved in a concentrated hydrobromic acid (HBr) to form a pale yellow solution. Then, the CsBr aqueous solution was added dropwise to the as-formed $PbBr_2$-HBr solution leading to orange precipitates. After filtering and washing, one can obtain pure phase $CsPbBr_3$ powder.[28] As shown in **Figure S1**, the XRD data is well consistent with a standard monoclinic phase of $CsPbBr_3$ (PDF#18-0364), and the scanning electron microscopy (SEM) image shows particles of micrometers in size. Additionally, the as-prepared $CsPbBr_3$ powder can dissolve in DSMO appearing as a transparent and colorless solution (middle panel of **Figure 1a**), making it possible to fabricate the corresponding thin film by simple one-step method. Interestingly, as shown in the middle images of **Figure 1a**, we can observe not only Tyndall effect but also a green emission when a blue laser (405 nm) passed through the as-prepared $CsPbBr_3$ precursor solution, indicating that it is a colloid solution containing some green-emitting particles. **Figure 1b** displays the PL spectra of DMSO and DMSO+$CsPbBr_3$ solution, where we can see that the DMSO solvent presents a broad emission with two peaks at 416 and 438 nm, showing strong blue luminescence for itself. While the DMSO+$CsPbBr_3$ solution reveals another broad green emission with peak at 558 nm, indicating that the green PL observed in **Figure 1a** is induced by $CsPbBr_3$. As shown in **Figure 1c**, the dynamic light scattering spectroscopy shows that the DMSO+$CsPbBr_3$ solution is a colloid solution with a very small average particle size (1.2 nm) and a narrow size distribution. After preparing the DMSO+$CsPbBr_3$ precursor solution, one can obtain $CsPbBr_3$ thin films by simply spin-coating this clear solution. **Figure 1d** shows a typical UV-Vis absorption and PL spectra of the as-deposited $CsPbBr_3$ thin film, the film exhibits a pronounced exciton absorption peak at 520 nm and a PL peak at 530 nm.

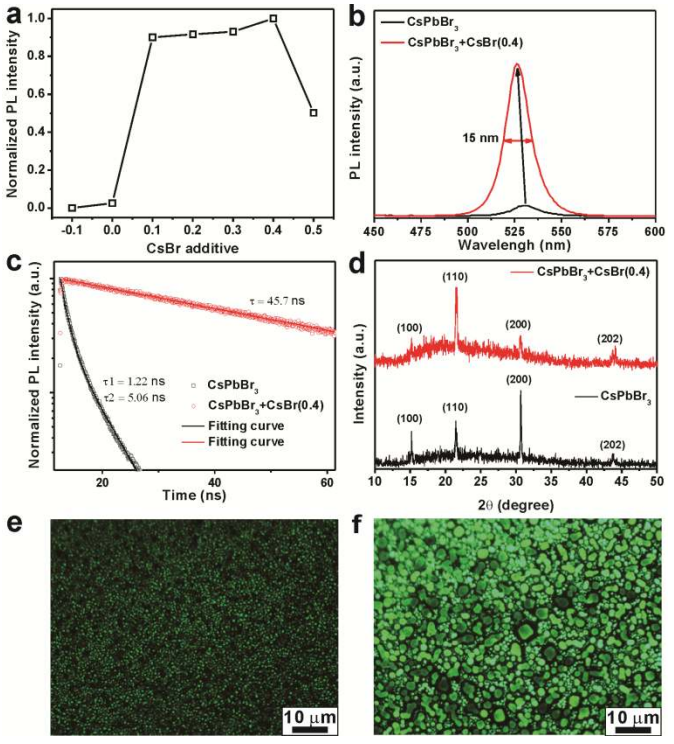

Figure 2. Compositional engineering of $CsPbBr_3$-based precursor solution for highly luminous perovskite films. (a) Normalized PL intensity versus CsBr

additive, indicating an optimized PL peak with 0.4 mole CsBr additive (represented as $CsPbBr_3$+CsBr(0.4)). (b) PL spectra, (c) time-resolved PL spectra and (d) XRD patterns of the pristine $CsPbBr_3$ and the optimized $CsPbBr_3$+CsBr(0.4) thin films. (e) and (f) fluorescence photographs of the pristine $CsPbBr_3$ and the optimized $CsPbBr_3$+CsBr(0.4) thin films.

The as-prepared $CsPbBr_3$ thin films have weak PL emission and we can barely observe the PL when the films were exposed to UV irradiance. We measured the absolute PLQY using an intergraded sphere to quantify the absorbed photons and emission photons. Then, the PLQY was calculated as the ratio of emission photons number and absorbed photons number. The PLQY was measured to be ~0.5 % for the as-prepared $CsPbBr_3$ film (**Figure S2**), which is not good enough for LEDs. As it has been proven that the optimized ratio of PbI_2 and MAI in the precursor solution for solar cells is not simply 1:1,[1, 29] we considered that the PL of $CsPbBr_3$ thin film can be possibly tuned by adding $PbBr_2$ or CsBr into the DMSO+$CsPbBr_3$ precursor solution. **Figure 2a** shows the PL intensity as a function of the CsBr additive amount, in which the positive X axis corresponds to CsBr additive amount while the negative value corresponds to $PbBr_2$ additive amount. Specifically, -0.1 represents a recipe of adding 0.1 mole of $PbBr_2$ to the as-prepared $CsPbBr_3$ (1 mole) precursor solution, and 0.2 on means adding 0.2 mole of CsBr to the as-prepared $CsPbBr_3$ (1 mole) precursor solution. It can be seen that adding some amount of $PbBr_2$ to the pristine $CsPbBr_3$ precursor solution will quench the PL of the corresponding perovskite film. By contrast, after adding some amount of CsBr into the precursor solution, the PL intensity of the corresponding perovskite films is significantly enhanced with an optimized CsBr additive of 0.4 mole, and the corresponding perovskite films are represented as $CsPbBr_3$+CsBr(0.4). However, CsBr additive of more than 0.4 mole will induce PL quenching. The PL spectra of the pristine $CsPbBr_3$ and $CsPbBr_3$+CsBr(0.4) thin films are shown **in Figure 2b**, where we observe that the CsBr additive significantly enhances the PL intensity and also induces a slight blue-shift in the emission peak (from 530 to 526 nm). To understand the reasons for PL enhancement induced by adding CsBr additive, time-resolved PL (TRPL) spectra were recorded and shown in **Figure 2c**. We observe that the TRPL curve of neat $CsPbBr_3$ film can be two-exponent fitted and the radiative recombination lifetime (τ_2) is 5.06 ns, similar to previous reports. [19, 20] And the TRPL curve of $CsPbBr_3$+CsBr(0.4) film can be one-exponent fitted well and the lifetime is 45.7 ns, which is nearly 4-10 times higher than the pure $CsPbBr_3$ film and other reports. [19, 20] Hence we propose that the Br-rich surface can passivate surface traps, reduce non-radiative recombination and result in PL enhancement, which is also consist with previous reports.[19] As shown in **Figure S2**, the PLQY of $CsPbBr_3$+CsBr(0.4) film is 33.6 %, which is 67 times higher than the pristine $CsPbBr_3$ thin film (0.5 %). The XRD data of the above two films are shown in **Figure 2d**, and for direct comparison, some other related standard diffraction patterns are shown in **Figure S3** and **S4**, from which we can see that both films indicate a monoclinic $CsPbBr_3$ phase (PDF#18-0364) and no CsBr residues observed. By comparing the XRD patterns especially the intensity change of peaks, we conclude that the CsBr additive induces a directional crystal growth along (110) facet, which may allow for plate-like morphology.

To probe the surface morphology of the as-prepared perovskite films, fluorescence photographs were recorded and presented in **Figure 2e** and **2f**. It is important to note that the images are not taken under the same intensity of UV excitation light. More specifically, the PL of the pristine $CsPbBr_3$ thin film is too weak to observe and need to be excited with 100 % of UV intensity, while the image of the $CsPbBr_3$+CsBr(0.4) film is taken with only 5 % of excitation UV intensity. Fluorescence microscopy suggests that the neat $CsPbBr_3$ film consists of polycrystalline islands smaller in size (hundreds of nanometer). By contrast, the $CsPbBr_3$+CsBr(0.4) film is made up of larger plate-like particles in the size of several micrometers, which is in agreement with the XRD data (**Figure 2d**). Another silent advantage of the as-prepared perovskite thin films is their outstanding ambient stability. As shown in **Figure S5**, the PL spectra of a $CsPbBr_3$+CsBr(0.4) film nearly remains the same even after storage in ambient air (~ 50 % humidity) for 3 months. It is believed that the big crystal size (micro-plates) may help to resist moisture penetration and improve stability.[30, 31]

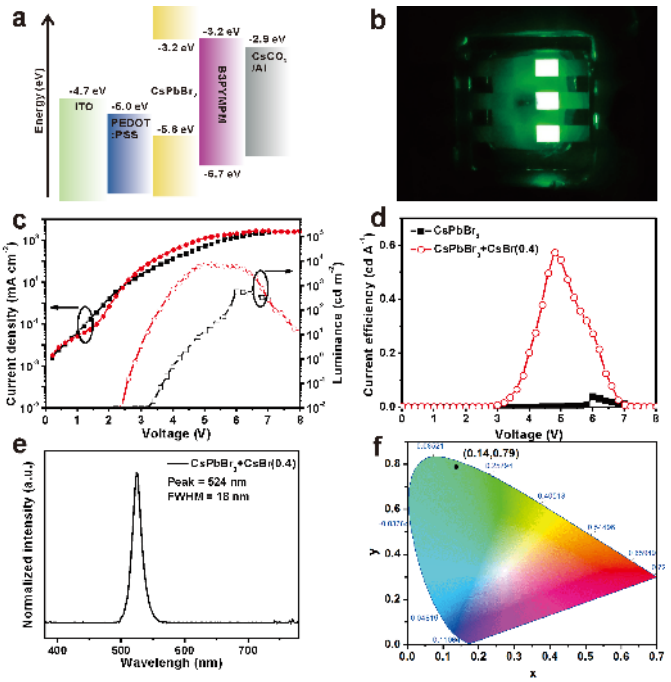

Figure 3. Fabrication and characterization of $CsPbBr_3$-based LEDs. (a) Energy level diagram and (b) photograph of the as-fabricated $CsPbBr_3$-based devices in operation. (c) Luminance-current density-voltage *(L-J-V)* curves and (d) current efficiency versus applied voltage (*CE-V*) curves of the as-fabricated LEDs. (e) Electroluminescence spectrum of the as-fabricated LED with an emission layer of $CsPbBr_3$+CrBr(0.4) film with an applied voltage of 4 V and (f) the corresponding CIE coordinates.

After the investigation of CsBr additive's effect on PL and morphology, the perovskite thin films were employed as emission layer and used to fabricate LEDs. **Figure 3a** schematically shows the energy level diagram of the as-fabricated LEDs and the corresponding cross sectional SEM

image is shown in **Figure S6**, where ITO glass serves as the anode, PEDOT:PSS acts as the hole transport layer (HTL) owing to its suitable work function (5.0 eV) and versatile process, B3PYMPM (4,6-Bis(3,5-di(pyridin-3-yl)phenyl)-2-methylpyrimidine) is used as the electron transport layer (ETL) as its conduction band matches the perovskite's conduction band well, and $CsCO_3$ is used as the buffer layer together with Al as the cathode for efficient electron injection. **Figure 3b** displays a photograph of the as-fabricated LEDs, revealing three uniform and bright emitting devices, each with an area of 2.0×1.5 mm^2. The top-view SEM images of the $CsPbBr_3$ and $CsPbBr_3$+CsBr(0.4) films deposited on PEDOT:PSS are shown in **Figure S7a** and **S7b,** respectively. As shown in **Figure S7a**, there are two kinds of polycrystalline domains observed in the as-fabricated $CsPbBr_3$ thin film, *i.e.*, dot-like small crystalline domains and sparse incomplete cuboid mircoparticles, and the surface coverage is poor due to the existence of cracks. It is noticeable that the surface morphology shown in **Figure S7a** is not ideal for LEDs application as the cracks will become the leakage points and reduce performance. By contrast, after adding some CsBr additive, **Figure S7b** shows a higher surface coverage with well-defined crystalline closely packed micro-cubes, which is good for LEDs application. To evaluate their LEDs performance, luminance-current density-voltage (*L-J-V*) curves were recorded and presented in **Figure 3c**. From *J-V* curves, we notice that the $CsPbBr_3$+CsBr(0.4) device shows a better diode characteristics and higher current density (beyond 2.5 V) than the pristine $CsPbBr_3$ device. We infer from the *L-V* curves that the pure $CsPbBr_3$ device shows a turn-on voltage (V_{on}) of 4.2 V and a maximum luminance of 567 cd m^{-2} at 6.0 V, which is similar to the previous reports.[4, 5, 20] The $CsPbBr_3$+CsBr(0.4) device reveals a much lower V_{on} of 2.8 V and a maximum luminance of 7,276 cd m^{-2} at 5.2 V, which are the lowest V_{on} and highest luminance reported in the literature, respectively. The low V_{on} may be attributed to better electron injection from ETL to perovskite due to the better energy alignment (**Figure 3a**). Meanwhile, performance of some other perovskite LEDs fabricated with different precursor solutions, like $CsPbBr_3$+CsBr(0.2) and *etc.*, are shown in **Figure S8**. It can be seen that the $CsPbBr_3$+CsBr(0.4) out-performs among all the devices, consistent with the previous PL optimization results (**Figure 2a**). **Figure 3d** shows the current efficiency (CE) versus applied voltage, indicating an improved CE from 0.04 cd A^{-1} without additives to 0.57 cd A^{-1} with additives. For direct comparison, some LEDs characteristics from our work and other related reports are summarized in **Table 1**, from which we can see that the performance shown here is among the best values reported, epically for the high luminance of 7,276 cd m^{-2}. **Figure 3e** presents the electroluminescence (EL) curve of a $CsPbBr_3$+CsBr(0.4) device with a driving voltage of 4.0 V, showing a symmetric emission peak at 524 nm with a FWHM of 18 nm, which is one of the narrowest values reported yet.[4] As shown in **Figure 3f**, the EL corresponds to Commission Internationale de l'Eclairage (CIE) color coordinates of (0.14,0.79), which is pure green.

Table 1. $CsPbBr_3$-based LEDs characteristics comparison of our work and other previous reports.

Reports	Emission material	V_{on} (V)	L_{max} (cd m^{-2})	CE_{max} (cd A^{-1})	Stability performance (T_{50}, min)
Yantara *et al.*[20]	planar film	3.0	407	0.035	N.A.
Song *et al.*[5]	NPs	4.2	946	0.43	N.A.
Zhang *et al.*[4]	NPs	3.5	1377	0.19	10 min in glovebox (V_{app} = 5 V)
Li *et al.*[7]	NPs	2.8	2335	0.28	N.A.
Our work	planar film	2.8	7276	0.57	Stable L>100 cd m^{-2} for > 15 h in ambient air (J_{app} = 66.67 mA cm^{-2})

NPs (nanoparticles) V_{on} (turn-on voltage), *L* (Luminance), CE (current efficiency), N.A. (not applicable), V_{app} (applied voltage) and J_{app} (applied current density).

Moreover, the external quantum efficiency (EQE) can be expressed as the ratio of emitted photons and charge carriers injected:

$$EQE = \frac{P_0/h\upsilon}{I/e}$$

where P_o is optical output power (measured by a calibrated photo-spectrometer), hυ is the photon energy at the emission frequency υ, *I* is the injection current, and e is the electron charge. By combining the performance result and EL spectra, the maximum EQE of the as-fabricated $CsPbBr_3$+CsBr(0.4) device is determined to be 0.15 %, which is also among the best performance reported.

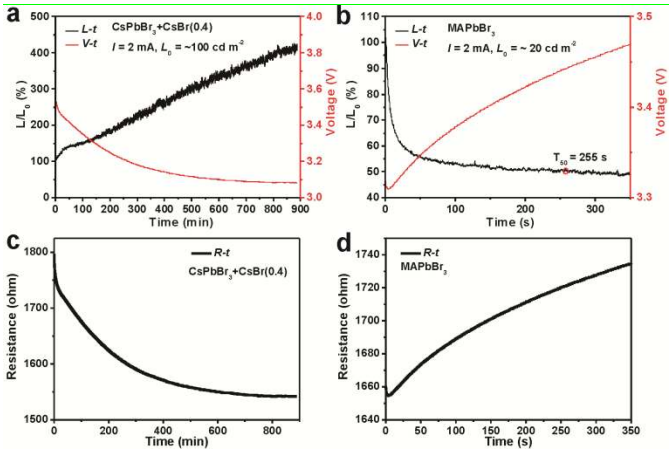

Figure 4. Ambient stability investigation of $CH_3NH_3PbBr_3$ and $CsPbBr_3$-based LEDs. (a) Relative luminance intensity versus time (*L-t*) and voltage versus time (*V-t*) characteristics of a $CsPbBr_3$-based LEDs with a constant driving current of 2 mA (corresponding to a current density of 66.67 mA cm^{-2}). (b) *L-T* and V-T characteristics of a $CH_3NH_3PbBr_3$-based LED tested under the same testing condition as $CsPbBr_3$-based LEDs (L_0: the starting luminance). (c) and (d) Resistance versus time (*R-t*) characteristics of the $CsPbBr_3$ and $MAPbBr_3$-based LEDs.

As mentioned above, the as-fabricated $CsPbBr_3$+CsBr(0.4) thin film showed an outstanding PL stability in ambient air (**Figure S5**). Hence, we believe that the corresponding LEDs

may perform well from a long-term stability point of view. To evaluate the ambient stability of the as-fabricated LEDs, we applied a constant current to the device and recorded the corresponding luminance intensity as a function of time. As well accepted, LEDs performance stability with an output of 100 cd m^{-2} is an important index for practical LEDs.[32] To evaluate our device stability, we therefore applied a constant current to the device, ensured the starting luminance is around 100 cd m^{-2} and recorded luminance output and applied voltage evolution as a function of time. As shown in the relative luminance intensity versus time (*L-t*) curve of **Figure 4a**, the $CsPbBr_3$+CsBr(0.4) device shows stable performance over more than 15 h under a constant driving current of 2 mA (*J* = 66.67 mA cm^{-2}) without any degradation but instead exhibits a steadily increasing luminance trend from around 100 to 400 cd m^{-2}. For direct comparison, a $MAPbBr_3$-based LED device was fabricated and tested under the same conditions, the corresponding *L-J-V* curve is shown in **Figure S9.** The as-fabricated $MAPbBr_3$-based LED shows a maximum luminance of 330 cd m^{-2} at 5 V, similar to the previous reports.[8, 9] However, when the device is driven with a constant current of 2 mA, as shown in **Figure 4b**, the luminance intensity decreases rapidly. We define half-lifetime (T_{50}) as the time for the luminance decreasing to 50 % of the starting luminance (L_0). Accordingly, T_{50} of the as-fabricated $MAPbBr_3$ device is only 255 s, which is still far from practical LEDs applications. As the applied current is fixed as 2 mA, so the voltage versus time (*V-t*) curves in **Figure 4a** and **4b** can be easily converted into *R-t* curves (resistance versus time) by equation of $R = V/I$. From the *R-t* curve shown in **Figure 4c**, we can see that the overall resistance of the $CsPbBr_3$+CsBr(0.4) device drops slightly with time. As there is not chemical reaction or phase transfer in the device, we propose that the decreasing of device resistance is due to interfaces contact improvement (ETL\Perovskite\HTL) or perovskite crystalline film annealing caused by joule heating annealing. And the decrease of device resistance (joule heating induced annealing effect) should be also the reason for the luminance increasing shown in **Figure 4a**. As the joule heat (Q) can be calculated with equation of $Q = I^2Rt$, and the *R-t* curve of the $MAPbBr_3$ device (**Figure 4d**) show that the resistance is growing, meaning that the device maybe overheated by the joule heat. As a result, we believe that the $MAPbBr_3$ perovskite will decompose due to the increasing joule heat. In other word, the instability of $MAPbBr_3$ device maybe attributed to the decomposition of $MAPbBr_3$ perovskites caused by joule heat under high current flowing.[33] By contrast, the $CsPbBr_3$ perovskites have been proved to be more thermal-stable compared to the common $MAPbBr_3$ perovskite,[16-18] which may contribute the superior device performance stability.

Besides evaluating LEDs stability at L_0 of 100 cd m^{-2}, we further investigated the device stability when it was operated at a higher luminance. As shown in **Figure S10**, when the applied current was increased to 10 mA, L_0 jumped to ~ 700 cd m^{-2}. However, the corresponding performance is not stable, as the initial luminance decrease to 60 % of L_0 in 100 min. Nonetheless, all our results unambiguously showed that the $CsPbBr_3$ LEDs can perform stably at least with L > 100 cd m^{-2}, which is definitely an important milestone in this field.

Conclusions

To conclude, we have successfully fabricated highly bright and durable $CsPbBr_3$-based LEDs, where the perovskite film is prepared by a simple one-step solution method in the ambient conditions. It is believed that the superior performance is attributed to the non-stoichiometric $CsPbBr_3$ precursor solution with CsBr additive, where the CsBr additive not only passivates the particle surface trap to enhance PLQY but also induces directional crystal growth to micro-plates. The as-fabricated highly luminous perovskite films, when applied as emitting layer in LEDs, show a record high brightness of 7,276 cd m^{-2} and excellent color purity (FWHM = 18 nm). According to the efficiency gaining process for inorganic/organic perovskite solar cell,[1, 2, 16] our developed one-step solution method is expected to continually improve LEDs performance by modifying the precursor solution. More importantly, the as-fabricated perovskite LEDs show incredible ambient stability with a luminance output > 100 cd m^{-2} (steady increase without any degradation trend) for at least 15 h, suggesting considerable potential promise towards developing practical LEDs for lighting and display.

Notes and references

‡ Acknowledgement: Q.H. Xiong gratefully acknowledges the strong support of this work from Singapore National Research Foundation through an Investigatorship Award (NRF-NRFI2015–03), Ministry of Education via two AcRF Tier 2 grants (MOE2013-T2-1-049 and MOE2015-T2-1-047) and Tier1 grant (2013-T1-002-232). H.V.D. is pleased to acknowledge Singapore National Research Foundation through an Investigatorship Award (NRF-NRFI2016-08) and Competitive Research Programme (CRP Award No. NRF-CRP14-2014-03).

1. D. Bi, W. Tress, M. I. Dar, P. Gao, J. Luo, C. Renevier, K. Schenk, A. Abate, F. Giordano, J. P. Correa Baena, J. D. Decoppet, S. M. Zakeeruddin, M. K. Nazeeruddin, M. Gratzel and A. Hagfeldt, *Sci Adv*, 2016, **2**, e1501170.
2. N. J. Jeon, J. H. Noh, W. S. Yang, Y. C. Kim, S. Ryu, J. Seo and S. I. Seok, *Nature*, 2015, **517**, 476-480.
3. W. Chen, Y. Wu, Y. Yue, J. Liu, W. Zhang, X. Yang, H. Chen, E. Bi, I. Ashraful, M. Gratzel and L. Han, *Science*, 2015, **350**, 944-948.
4. X. Zhang, H. Lin, H. Huang, C. Reckmeier, Y. Zhang, W. C. Choy and A. L. Rogach, *Nano Lett*, 2016, **16**, 1415-1420.
5. J. Song, J. Li, X. Li, L. Xu, Y. Dong and H. Zeng, *Adv Mater*, 2015, **27**, 7162-7167.
6. J. Wang, N. Wang, Y. Jin, J. Si, Z. K. Tan, H. Du, L. Cheng, X. Dai, S. Bai, H. He, Z. Ye, M. L. Lai, R. H. Friend and W. Huang, *Adv Mater*, 2015, **27**, 2311-2316.
7. G. Li, F. W. Rivarola, N. J. Davis, S. Bai, T. C. Jellicoe, F. de la Pena, S. Hou, C. Ducati, F. Gao, R. H. Friend, N. C. Greenham and Z. K. Tan, *Adv Mater*, 2016, **28**, 3528-3534.
8. G. Li, Z. K. Tan, D. Di, M. L. Lai, L. Jiang, J. H. Lim, R. H. Friend and N. C. Greenham, *Nano Lett*, 2015, **15**, 2640-2644.

9. Z. K. Tan, R. S. Moghaddam, M. L. Lai, P. Docampo, R. Higler, F. Deschler, M. Price, A. Sadhanala, L. M. Pazos, D. Credgington, F. Hanusch, T. Bein, H. J. Snaith and R. H. Friend, *Nature nanotechnology*, 2014, **9**, 687-692.
10. H. Cho, S.-H. Jeong, M.-H. Park, Y.-H. Kim, C. Wolf, C.-L. Lee, J. H. Heo, A. Sadhanala, N. Myoung, S. Yoo, S. H. Im, R. H. Friend and T.-W. Lee, *Science*, 2015, **350**, 1222-1225.
11. Y. H. Kim, H. Cho, J. H. Heo, T. S. Kim, N. Myoung, C. L. Lee, S. H. Im and T. W. Lee, *Adv Mater*, 2015, **27**, 1248-1254.
12. H. Chen, Z. Wei, H. He, X. Zheng, K. S. Wong and S. Yang, *Adv Energy Mater*, 2016, **6**, n/a-n/a.
13. Z. Wei, X. Zheng, H. Chen, X. Long, Z. Wang and S. Yang, *J. Mater. Chem. A*, 2015, **3**, 16430-16434.
14. Z. Wei, H. Chen, K. Yan and S. Yang, *Angew Chem Int Ed Engl*, 2014, **53**, 13239-13243.
15. Z. Wei, K. Yan, H. Chen, Y. Yi, T. Zhang, X. Long, J. Li, L. Zhang, J. Wang and S. Yang, *Energy Environ. Sci.*, 2014, **7**, 3326-3333.
16. M. Saliba, T. Matsui, J.-Y. Seo, K. Domanski, J.-P. Correa-Baena, M. K. Nazeeruddin, S. M. Zakeeruddin, W. Tress, A. Abate, A. Hagfeldt and M. Grätzel, *Energy Environ. Sci.*, 2016, **9**, 1989-1997.
17. R. J. Sutton, G. E. Eperon, L. Miranda, E. S. Parrott, B. A. Kamino, J. B. Patel, M. T. Hörantner, M. B. Johnston, A. A. Haghighirad, D. T. Moore and H. J. Snaith, *Adv Energy Mater*, 2016, DOI: 10.1002/aenm.201502458, n/a-n/a.
18. D. P. McMeekin, G. Sadoughi, W. Rehman, G. E. Eperon, M. Saliba, M. T. Hörantner, A. Haghighirad, N. Sakai, L. Korte, B. Rech, M. B. Johnston, L. M. Herz and H. J. Snaith, *Science*, 2016, **351**, 151-155.
19. X. Li, Y. Wu, S. Zhang, B. Cai, Y. Gu, J. Song and H. Zeng, *Adv Funct Mater*, 2016, DOI: 10.1002/adfm.201600109, n/a-n/a.
20. N. Yantara, S. Bhaumik, F. Yan, D. Sabba, H. A. Dewi, N. Mathews, P. P. Boix, H. V. Demir and S. Mhaisalkar, *J Phys Chem Lett*, 2015, **6**, 4360-4364.
21. Y. Deng, E. Peng, Y. Shao, Z. Xiao, Q. Dong and J. Huang, *Energy Environ. Sci.*, 2015, **8**, 1544-1550.
22. N. J. Jeon, J. H. Noh, Y. C. Kim, W. S. Yang, S. Ryu and S. I. Seok, *Nat Mater*, 2014, **13**, 897-903.
23. M. Kulbak, D. Cahen and G. Hodes, *The Journal of Physical Chemistry Letters*, 2015, DOI: 10.1021/acs.jpclett.5b00968, 2452-2456.
24. L. Protesescu, S. Yakunin, M. I. Bodnarchuk, F. Krieg, R. Caputo, C. H. Hendon, R. X. Yang, A. Walsh and M. V. Kovalenko, *Nano Lett*, 2015, **15**, 3692-3696.
25. G. Nedelcu, L. Protesescu, S. Yakunin, M. I. Bodnarchuk, M. J. Grotevent and M. V. Kovalenko, *Nano Lett*, 2015, **15**, 5635-5640.
26. Q. A. Akkerman, V. D'Innocenzo, S. Accornero, A. Scarpellini, A. Petrozza, M. Prato and L. Manna, *J Am Chem Soc*, 2015, **137**, 10276-10281.
27. J. Burschka, N. Pellet, S. J. Moon, R. Humphry-Baker, P. Gao, M. K. Nazeeruddin and M. Gratzel, *Nature*, 2013, **499**, 316-318.
28. C. C. Stoumpos, C. D. Malliakas, J. A. Peters, Z. Liu, M. Sebastian, J. Im, T. C. Chasapis, A. C. Wibowo, D. Y. Chung, A. J. Freeman, B. W. Wessels and M. G. Kanatzidis, *Cryst Growth Des*, 2013, **13**, 2722-2727.
29. Y. C. Kim, N. J. Jeon, J. H. Noh, W. S. Yang, J. Seo, J. S. Yun, A. Ho-Baillie, S. Huang, M. A. Green, J. Seidel, T. K. Ahn and S. I. Seok, *Adv Energy Mater*, 2015, DOI: 10.1002/aenm.201502104, n/a-n/a.
30. J. H. Kim, S. T. Williams, N. Cho, C. C. Chueh and A. K. Y. Jen, *Adv Energy Mater*, 2015, **5**, n/a-n/a.
31. Z. Yang, C.-C. Chueh, F. Zuo, J. H. Kim, P.-W. Liang and A. K. Y. Jen, *Adv Energy Mater*, 2015, DOI: 10.1002/aenm.201500328, n/a-n/a.
32. X. Dai, Z. Zhang, Y. Jin, Y. Niu, H. Cao, X. Liang, L. Chen, J. Wang and X. Peng, *Nature*, 2014, **515**, 96-99.
33. J. C. Yu, D. W. Kim, D. B. Kim, E. D. Jung, J. H. Park, A. Y. Lee, B. R. Lee, D. Di Nuzzo, R. H. Friend and M. H. Song, *Adv Mater*, 2016, DOI: 10.1002/adma.201601105, n/a-n/a.

